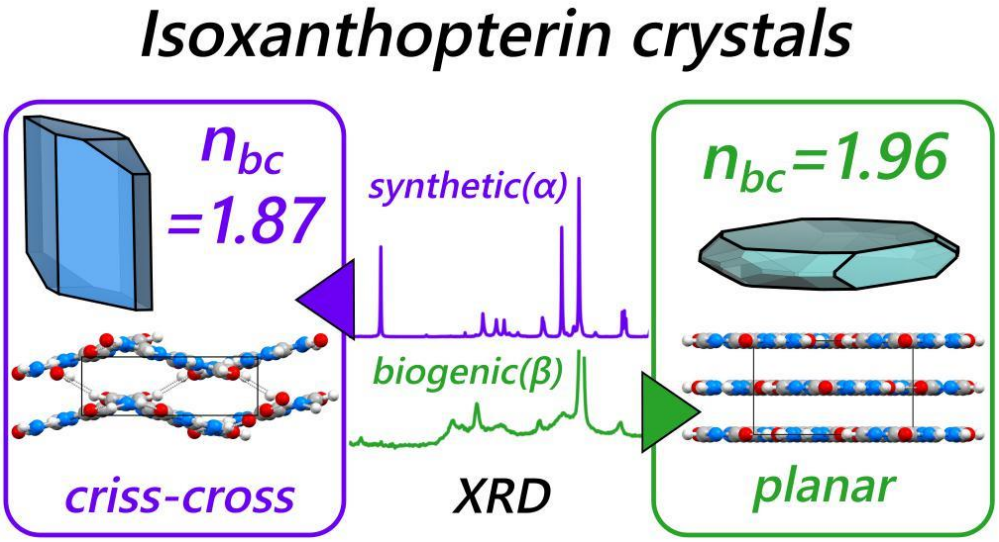
Isoxanthopterin crystals
n_{bc} =1.87
criss-cross
synthetic(α)
biogenic(β)
XRD
n_{bc}=1.96
planar

Structure and morphology of light-reflecting synthetic and biogenic polymorphs of isoxanthopterin: A comparison

Anna Hirsch,[1] Benjamin A. Palmer,[2] Ashwin Ramasubramaniam,[3] P. Andrew Williams,[4] Kenneth D. M. Harris,[4] Boaz Pokroy,[5] Steve Weiner,[2] Lia Addadi,[2] Leslie Leiserowitz[1], Leeor Kronik[1]

[1]*Department of Materials and Interfaces, Weizmann Institute of Science, Rehovoth 7610001, Israel*
[2]*Department of Structural Biology, Weizmann Institute of Science, Rehovoth 7610001, Israel*
[3]*Department of Mechanical and Industrial Engineering, University of Massachusetts Amherst, Amherst, Massachusetts 01003, U.S.A*
[4]*School of Chemistry, Cardiff University, Park Place, Cardiff, CF10 3AT, U.K.*
[5]*Department of Materials Science and Engineering and the Russell Berrie Nanotechnology Institute, Technion - Israel Institute of Technology, Haifa 32000, Israel*

Abstract

Until recently it was thought that the only optical function of pteridines in biology was to act as light-absorbing pigments, but a recent report by some of us revealed that crystalline isoxanthopterin is a reflector in the eyes of decapod crustaceans. Here, we report the formation of crystalline isoxanthopterin synthetically from the polar dimethyl sulfoxide (DMSO) solvent, with X-ray diffraction analysis revealing a crystal structure different from that of biogenic isoxanthopterin. The structure of the new polymorph was determined in two independent ways. In one approach, it was generated and optimized using first principles calculations, followed by comparison of simulation and experiment for high-resolution powder X-ray diffraction (PXRD) and electron diffraction. In the other approach, the structure was obtained definitively from PXRD data using a direct-space genetic algorithm for structure solution followed by Rietveld refinement. The synthetic structure is different from its biogenic counterpart, especially in having a non-planar criss-cross H-bonded arrangement. We also rationalized the morphology of the crystals and the effect of the DMSO thereon, via a comparison between observed and theoretical growth morphologies. In addition, we calculated the optical properties of the synthetic structure and found its two dominant refractive indices to be somewhat lower than those of its biogenic counterpart, but still as high as those of reflecting guanine crystals. Synthetic isoxanthopterin therefore emerges as a promising candidate for incorporation in artificial optical systems.

I. Introduction

Isoxanthopterin belongs to the pteridine family of molecules, which are heterocyclic compounds composed of fused pyrimidine and pyrazine rings (Scheme **1a)**. Historically, it was thought that the exclusive optical function of pteridines[1] in nature was as light-absorbing pigments, associated with yellow/red xanthophore pigment cells.[2] However, a recent report by some of us revealed that crystalline isoxanthopterin is the reflective material in the mirrored eyes of decapod crustaceans such as lobsters, shrimp, crayfish, and prawns.[3] This study provided conclusive evidence to substantiate the suggestion that pteridines also function as reflective materials in nature.[4–6] By comparison, the most widely known crystalline light reflective material in biological systems is guanine,[7] which is a heterocyclic purine composed of fused imidazole and pyrimidine rings (Scheme **1b)**. Crystalline guanine has been found in many different organisms, in which the reflecting crystals have different sizes and shapes and fulfill different functions both in structural coloration and vision.[8–12]

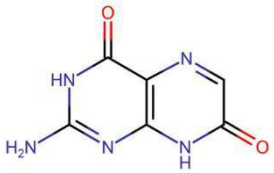

1a Isoxanthopterin

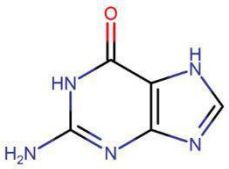

1b Guanine

The aforementioned study[3] characterized the hierarchical superstructure and optical properties of the "superposition compound eye" of decapod crustaceans.[13] Identification and structural elucidation of the biogenic crystalline isoxanthopterin in crustacean eyes was extremely challenging owing to the crystal's nanoscopic size, location within the tissue, and stability. Only a combination of *in-situ* diffraction and spectroscopic techniques, combined with crystal structure generation and optimization via first principles computations, allowed a full characterization of the crystal structure and properties. Computational analysis predicts an extremely high refractive index of biogenic isoxanthopterin crystals (n = 1.96), revealing that isoxanthopterin is an excellent choice for reflective optics, even outshining biogenic guanine crystals (n = 1.83).[14]

The discovery of the extraordinary optical properties of biogenic isoxanthopterin crystals stimulated us to try to obtain isoxanthopterin crystals by synthetic methods.

Indeed, the high refractive index of isoxanthopterin, together with the fact that it is a nonhazardous material, make it a promising candidate for incorporation into artificial optical systems. In fact, biogenic guanine is already used as a reflective material in a variety of commercial products, such as cosmetics, paints, and jewelery.[15,16] Recently, guanine was also incorporated into sophisticated systems with dynamic control over crystal orientation, providing magnetically tunable reflectivity.[17–19]

Importantly, the crystal structure and morphology of synthetic isoxanthopterin could be different from that of the biogenic crystal, as polymorphism is a common phenomenon in biomineralization in both inorganic[20–24] and organic[25–28] systems. Indeed, synthetic -guanine[29] has the same layer structure as the biogenic -form,[25] but has a different interlayer arrangement and is marginally more stable.[30] Nonetheless, all biogenic guanine samples examined to date were found in the -form.

Here, we present a new synthetic form of isoxanthopterin and report its crystal structure, which is different from that of its biogenic counterpart. We describe the crystal structure of the new synthetic form in terms of molecular arrangement, intermolecular interactions, crystal symmetry, crystal morphology, and optical properties. Furthermore, we compare and contrast these properties with those of the biogenic form of isoxanthopterin.

II. Materials and Methods

1. Materials

Synthetic crystals of anhydrous isoxanthopterin (hereafter denoted the α-polymorph) were prepared by crystallization from anhydrous dimethyl sulfoxide (DMSO) using the following method, adapted from a previous report by Levy-Lior *et al.*[31] Isoxanthopterin (in powder form, purchased from Sigma Aldrich) was dissolved in hot DMSO at 90 °C (typical concentration, 0.4 mg/ml) with vigorous stirring. Once dissolution was complete, the hot solution was filtered and gradually cooled to room temperature. The solution was then left at room temperature in a conical flask with puncture holes in the lid, allowing slow evaporation of the DMSO. After several weeks, crystals of isoxanthopterin were observed. The crystal suspension was then centrifuged for 1 hr at 14,000 rpm, producing a crystal-pellet at the base of the Eppendorf tube. The supernatant was removed and replaced with

absolute ethanol or double-distilled water (DDW). The pellet was re-dispersed and centrifuged using the same conditions twice. The crystals were stored in either ethanol or DDW until required for further analysis.

2. Synchrotron high resolution powder X-ray diffraction (HR-PXRD)

Synchrotron HR-PXRD was used in order to collect high quality PXRD data, recorded on the ID22 high-resolution powder diffraction beamline of the European Synchrotron Radiation Facility (ESRF, Grenoble, France), with λ= 0.41066 Å at ambient temperature. Instrument calibration was performed by using NIST silicon standards, final instrumental contribution to the full width at half maximum (FWHM) did not exceed 0.004^{o} 2θ.[32] The samples were inserted in a spinning 1 mm diameter borosilicate capillary and the diffracted beam was monochromatized and collected by means of a multianalyzer stage equipped with a nine-point detector (for further information, http://www.esrf.eu/id22/technical-description).

3. Transmission Electron Microscopy (TEM) imaging and diffraction

From a suspension of synthetically-produced crystals of the α polymorph of isoxanthopterin (in DDW), a drop was removed and applied to a glow-discharged homemade carbon-coated, copper TEM grid. The suspension was allowed to settle for 45 s and blotted. Samples were observed with an FEI Tecnai T12 transmission electron microscope operated at 120 kV. Images and diffraction patterns were recorded on a Gatan OneView camera using imaging and diffraction modes respectively.

4. Structure determination directly from PXRD data

PXRD data for the synthetic polymorph of isoxanthopterin were recorded at ambient temperature on a Bruker D8 instrument (CuK $_1$ radiation; primary-beam Ge monochromator) operating in transmission mode, with the sample contained in a glass capillary (2 range, 3.35° – 70.00°; step size, 0.017°; data collection time, 62 hr).

Structure determination was carried out directly from the PXRD data using methodology described in ref. [33]. The PXRD pattern was indexed using the TREOR code[34] in the CRYSFIRE program suite,[35] giving the following unit cell with orthorhombic metric

symmetry: a = 4.49 Å, b = 9.89 Å, c = 15.38 Å, V = 682.5 Å^3. Density considerations suggest that the unit cell contains four molecules of isoxanthopterin. Initially, profile fitting and unit cell refinement were based on orthorhombic metric symmetry, using the Le Bail method[36] in the GSAS program[37] over the range 4° ≤ 2 ≤ 70°, producing a good fit between the experimental and calculated PXRD data (R_{wp} = 1.95%, R_p = 1.41%).

Structure solution was carried out from the PXRD data using the direct-space genetic algorithm (GA) technique in the program EAGER.[38–43] Initial GA structure solution calculations were carried out for several different orthorhombic and monoclinic space groups, but structurally sensible results were obtained only for space group $P2_1/n$. In the GA structure solution calculations for $P2_1/n$, the asymmetric unit comprised one molecule of isoxanthopterin, constructed using standard bond lengths and bond angles, with each trial structure defined by six structural variables (three positional variables and three orientational variables). In total, 16 independent GA calculations were carried out for space group $P2_1/n$ (each calculation involved the evolution of 100 generations for a population of 100 structures, with 10 mating operations and 50 mutation operations per generation). The 16 independent GA calculations resulted in the same structure with lowest powder-profile R-factor R_{wp} (representing the best agreement between experimental and calculated PXRD data).

On recognizing that the structure is monoclinic, profile fitting and unit cell refinement were repeated using the Le Bail procedure in space group $P2_1/n$, giving a better quality of fit (R_{wp} = 1.85%, R_p = 1.36%) than that obtained for orthorhombic metric symmetry.

The best trial structure obtained in the GA structure solution calculations was subjected to geometry optimization using periodic dispersion-augmented density functional theory (DFT) calculations with fixed unit cell (carried out by the PBE+TS-vdW approach described in the next sub-section, using CASTEP[44] version 8.0 with ultrasoft pseudopotentials). The geometry-optimized structure was used as the starting structural model for Rietveld refinement, carried out in space group $P2_1/n$ using the GSAS program. Restraints (based on the molecular geometry of the DFT-optimized structure) were applied to bond lengths and bond angles, and planar restraints were applied to the whole molecule. A common isotropic displacement parameter was refined for the non-hydrogen atoms. The isotropic displacement parameter for hydrogen atoms was set as 1.2 times the refined

isotropic displacement parameter for the non-hydrogen atoms. The final Rietveld refinement gave excellent fit to the experimental PXRD data (R_{wp} = 1.88%, R_p = 1.38%), comparable to the quality of fit obtained in the profile-fitting procedure, with final refined parameters: a = 4.4848(6) Å, b = 9.8986(13) Å, c = 15.3735(20) Å, β = 90.061(11)°, V = 682.48(19) Å^3 (2θ range, 4° – 70°; 3866 profile points; 72 refined variables). The final refined crystal structure, following transformation to the specific $P2_1/c$ setting used in the structure prediction component of the present work (see Section III), is deposited as a cif file in Supporting Information.

5. Computational Details

Electronic structures, total energies, and geometries were calculated by solving the Kohn-Sham equations of DFT within the generalized gradient approximation (GGA), using the Perdew, Burke and Ernzerhof (PBE) exchange-correlation functional.[45] The total energy was augmented by Tkatchenko-Scheffler van der Waals (TS-vdW) pair-wise dispersive terms.[46] All calculations were carried out using the Vienna Ab Initio Simulation Package (VASP)[47] plane wave basis code, in which TS-vdW dispersive corrections were implemented.[48,49] The ionic cores were described by the projected augmented wave (PAW) method.[47,50]

The planewave energy cutoff used for the calculations was 900 eV. For the monoclinic symmetry polymorphs, a 6 2 1 *k*-point grid sampling of the Brillouin zone was used and for the orthorhombic symmetry polymorph a 3 2 1 grid was used. The *k*-point grids result in similar mesh density because in the orthorhombic polymorph the length of the *a* axis is approximately twice that of the *d*(100) spacing of the monoclinic polymorph. Atomic forces in the system were relaxed to 10^{-4} eV/Å and stress was relaxed to 10^{-2} kB. We note that in the geometry optimization process of the synthetic isoxanthopterin structure, a less-stringent force convergence criterion of 10^{-2} eV/Å produced a layered structure that remained almost planar. However, once the convergence criterion for the forces was tightened such that all forces in the system were driven below 10^{-4} eV/Å, changes in planarity occurred until the final structure was obtained.

For the calculation of the refractive index, the static ion-clamped dielectric matrix was calculated using density functional perturbation theory including local-field effects at the

Hartree level.[51,52] For this calculation, finer *k*-point grids were used, corresponding to 9 3 2 for monoclinic symmetry and 7 4 2 for orthorhombic symmetry.

Molecular structures were visualized using the Mercury CSD program, the Materials Studio visualizer, and the VESTA[53] program. The same atomic color code is used throughout (oxygen, red; nitrogen, blue; carbon, gray; hydrogen, white; sulfur, yellow). Hydrogen bonds are marked by dashed lines.

PRXD patterns of the computationally generated polymorphs were simulated using Materials Studio Reflex module 6.1. Broadening of the PXRD profile was done following the Pseudo-Voigt model. The simulated ED patterns were obtained using the CrystalMaker (2.7.7) - SingleCrystal program (2.2.9). The sizes of reciprocal lattice reflections were scaled in proportion to the corresponding observed intensity.

The theoretical morphologies of the synthetic and biogenic crystal structures were obtained using the Materials Studio Morphology module 6.1. The crystal shape was simulated by use of the "growth morphology" or the "equilibrium morphology".[54–56] Growth morphology assumes that the growth rate of the crystal face is proportional to its attachment energy, which is defined as the energy released on attachment of a growth slice to a growing crystal surface.[57] Thus, the faces with lowest attachment energy are the slowest growing and, therefore, have the greatest morphological importance. The equilibrium morphology is determined by the minimum of the surface free energy. If the surface free energies are known for all relevant crystal faces, the morphology of a crystal in equilibrium with its surroundings can be visualized using a Wulff construction. Attachment energies and surface energies[58] were calculated using the Dreiding forcefield,[59] which is considered to be sufficient for organic, biological and main-group inorganic materials. It is important to note that the morphology simulation method does not take into account factors such as the presence or absence of solvents or excipients and possible surface reconstructions, which can have a profound influence on experimentally observed morphologies, as observed in the present study (see below).

To model the experimentally observed morphologies (Figure 6B,C,D,E(iii)) for each crystal shape, the relevant growth faces were chosen from a list of all possible growth faces obtained by the Bravais-Friedel-Donnay-Harker (BFDH) method.[55] The specific crystal shape was generated by manipulating the relevant lattice distance d_{hkl} of the growth faces

{*hkl*} in order to modify its morphological importance, until an observed similarity was reached. The similarity between the modeled and observed shape allows an easy labeling and identification of the various experimentally exhibited faces.

III. Results

Crystal structure determination of synthetic isoxanthopterin

Pteridines are typically characterized by low solubility in aqueous media and common organic solvents and are difficult to crystallize.[60] Given the structural similarity between the guanine and isoxanthopterin molecules, we utilized the approach applied previously for precipitation of synthetic guanine, in which crystals were obtained from aqueous solutions at different pH values[30] or from polar dimethyl sulfoxide (DMSO).[31] The latter method proved successful in producing anhydrous crystalline isoxanthopterin, as a microscopic powder. PXRD data of the obtained synthetic crystals are shown in

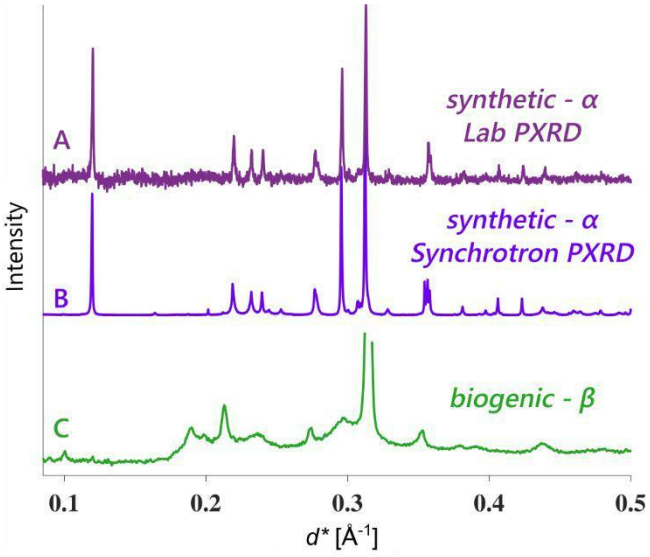

Figure 1, where they are compared to previously collected XRD data for the biogenic polymorph. Clearly, the synthetic form is different from that of the biogenic analogue. We label the structure of the synthetic crystals as the α-polymorph, and that of the biogenic crystals as the β-polymorph.

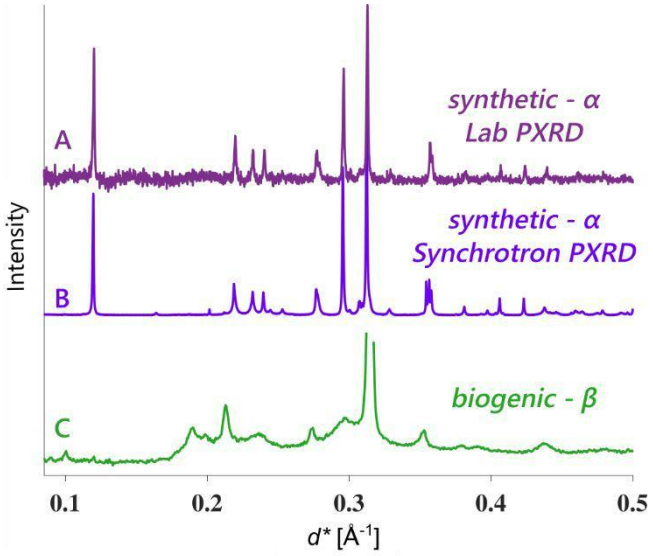

Figure 1 Lab PXRD (A) and Synchrotron PXRD (B) data for the synthetic (α) isoxanthopterin polymorph, compared to *in situ* XRD data for the biogenic (β) isoxanthopterin polymorph, reproduced from Ref. [3]. In C, the intensity of the strongest reflection was truncated to make all reflections more visible.

In our previous description of the determination of the crystal structure of biogenic isoxanthopterin,[3] we generated several possible crystalline arrangements *in silico*, using an approach similar to that reported previously for prediction of the crystal structure of biogenic guanine.[25] Both guanine and isoxanthopterin are planar conjugated molecules with numerous H-bond donor and acceptor sites. Therefore, the generation of a crystal structure relied on the assumption that the structure is dominated by intermolecular H-bonding and close-packing interactions. In order to generate the H-bonding motif of isoxanthopterin, we noted that the molecule embodies four NH donors, one CH donor, and six lone-pair electron lobes. We first envisaged the formation of a cyclic centrosymmetric dimer, shown in Figure 2A, containing four H-bonds (two NH···N and two NH···O), as the basic building block of a possible molecular arrangement. This is the same building block for both the synthetic and biogenic structures. We then took advantage of the H-bonding complementarity between the two adjacent sides of the isoxanthopterin molecule to form a two-dimensional H-bonding array by twofold screw (2_1) and glide (*c*) symmetries. This generated a unique layer of symmetry $2_1/c$, in which all H-bonds are satisfied (Figure 2A).

We next generated different interlayer packing motifs, via monoclinic and orthorhombic symmetries. These crystal structures were then optimized using dispersion-

augmented DFT, and the corresponding PXRD patterns were calculated. The DFT structural optimization of the orthorhombic structure maintained perfect planarity, yielding the rarely observed high symmetry space group *Cmce*, which has *Pbca* symmetry with an additional mirror (*m*) symmetry element. The computed PXRD pattern for this structure agreed very well with experimental data for the biogenic β-polymorph.[3]

DFT optimization of the monoclinic arrangement with a translational offset between layers along the *c* axis, as presented in this report, brought about a significant change to the structure, most notably a loss of coplanarity. Detailed examination of the non-planar arrangement (Figure 2B) reveals a new motif binding the H-bonded dimers, in which they are interlinked by CH···O bonds via inversion ($\bar{1}$) symmetry, forming criss-cross *ribbons* along the diagonals $a \pm b$ (see Figure 2C,D), with the isoxanthopterin molecules tilted by ~ ±23º with respect to the *bc* plane. We note that a CH···O=C cyclic bonding motif[61] is observed in other structures, particularly 1,4-benzoquinones[62,63] and carboxylic acids.[62] The neighboring ribbons, stacked along the *a*-axis are juxtaposed along the *c* axis, and interconnected by NH···O and NH···N bonds, (Figure 2B). The computed PXRD pattern for this structure (Figure 3A), following refinement of lattice parameters, agrees very well with the experimental peak positions of the synchrotron PXRD data obtained from synthetic samples of α-isoxanthopterin (Figure 3B), with some remaining differences in intensity, but disagrees completely with the computed PXRD pattern for the biogenic polymorph (Figure 3C), in agreement with the experimental results.

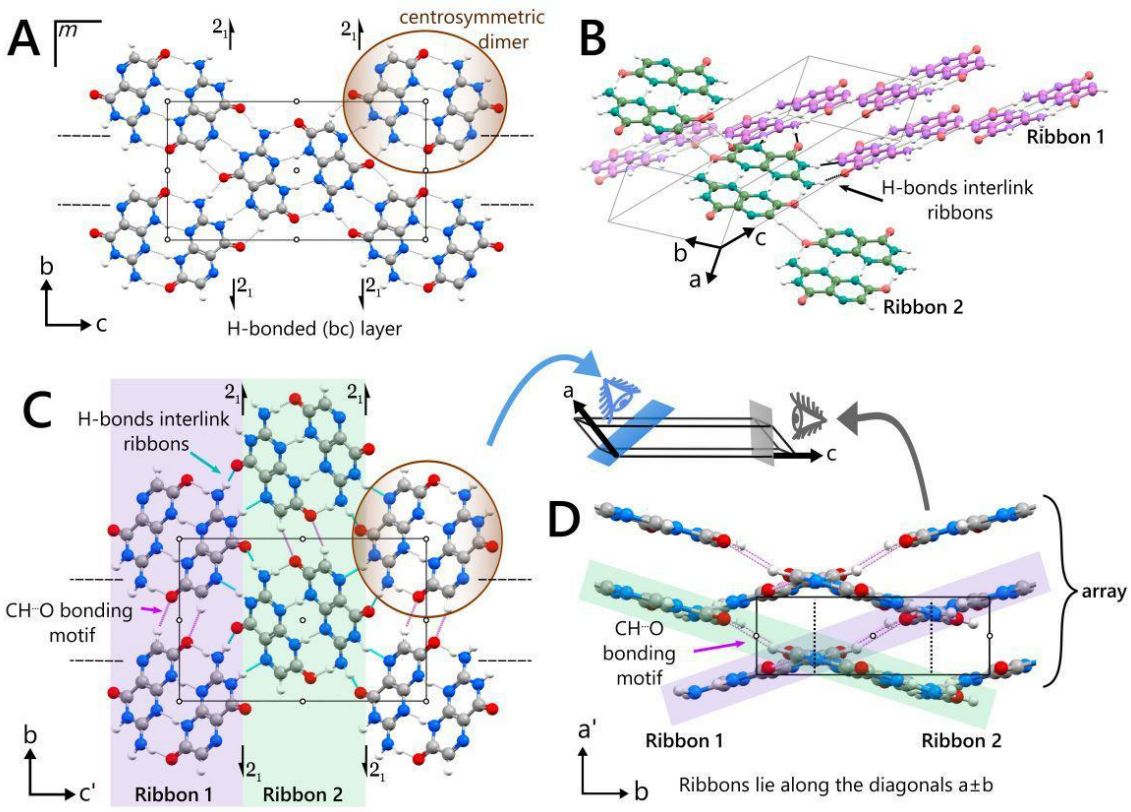

Figure 2 (A) H-bonded layer motif in the biogenic β-polymorph of isoxanthopterin. (B-D) H-bonding motif in the synthetic α-polymorph of isoxanthopterin, with neighboring criss-cross ribbons highlighted in purple and green. (B) An oblique view of the three-dimensional network of the H-bonded arrangement. (C) View along the *a* axis, with the length of projection axis given by $c'=c\cdot\sin\beta$. (D) Criss-cross arrangement of H-bonded ribbons viewed along the *c* axis, where the length of the projection is $a'=a\cdot\sin\beta$.

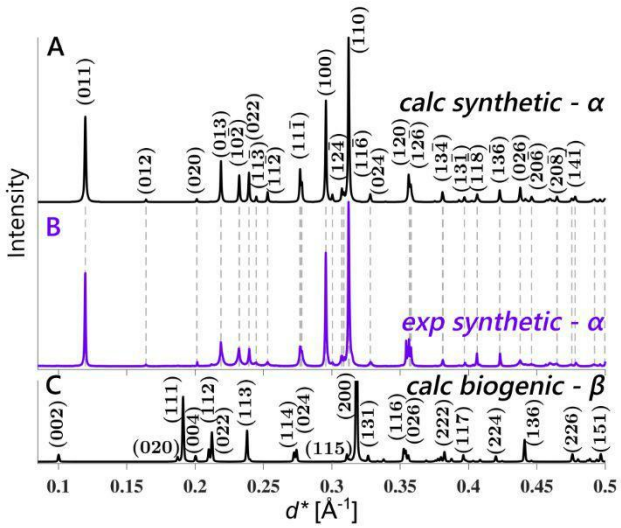

Figure 3 Measured synchrotron PXRD pattern of the synthetic isoxanthopterin polymorph (B), compared to computed patterns of the (A) synthetic (α) and (C) biogenic (β) isoxanthopterin polymorphs. In (A), the data are based on a lattice-parameter refinement analysis of the calculated structure. In (C), the intensity of the (200) reflection is truncated for clarity.

Definitive evidence in support of the structure presented in Figure 2B-D was obtained by a completely independent determination of the structure directly from PXRD data, using the approach described in Section II.4. The final lattice parameters obtained from the Rietveld refinement of this structure are given (following transformation to the $P2_1/c$ setting) in Table 1, where they are additionally compared to those obtained from the computational approach, as well as to the lattice parameters of the biogenic polymorph. The results from the final Rietveld refinement, shown in Figure 4, clearly indicate excellent agreement between experimental and calculated PXRD data (R_{wp} = 1.88%, R_p = 1.38%), with a quality of fit comparable to that obtained in the profile-fitting calculation using the Le Bail method (R_{wp} = 1.85%, R_p = 1.36%).

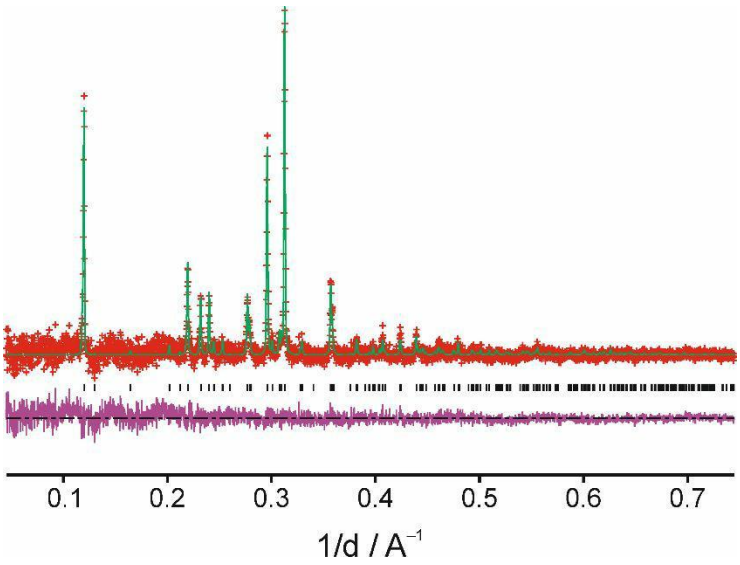

Figure 4 Final Rietveld refinement for the synthetic polymorph of isoxanthopterin. Red "+" marks, experimental data; green line, calculated data; black tick marks, predicted peak positions; magenta line (at bottom), difference between experimental and calculated powder XRD patterns.

The above considerations fully establish the crystal structure of the synthetic α-polymorph, with excellent agreement between *in silico* and PXRD-based structure determination. This excellent agreement is further demonstrated in Figure 5, where the computationally predicted and experimentally determined structures are overlaid. Having achieved that, the three-dimensional H-bonded network in the crystal structure merits further discussion, because it determines the space-group symmetry and unit cell dimensions, as given in Table 1. In the computed structure, the computed repeat distance of the planar H-bonded ribbon along the diagonals $a \pm b$ is 11.0 Å (Figure 2D). These ribbons cannot form an extended coplanar H-bonded layer as in the biogenic form (Figure 2A). Rather, they are stacked along the short *a* axis into extended *arrays* in the *ab* plane, which are juxtaposed along the *c* axis, separated by 10.1 Å (equivalent to *c*/2), as generated by the *c*-glide. The length of the resulting *c*-axis (20.2 Å) is almost equal to the corresponding axis of the computed biogenic β form (20.0 Å). However, the 10.1 Å length of the *b* axis of the synthetic α form is 0.6 Å shorter than the corresponding *b* axis of the β-polymorph (10.7 Å). This shorter length induces the juxtaposed arrays to form a three-dimensional network of NH···N and NH···O bonds via 2_1 symmetry, relating nearest neighbor molecules of the criss-cross ribbons (Figure 2D). The interplay between the

constraints imposed on the lengths and orientations of the *b* axis and the diagonal $a \pm b$ axes by the H-bond network fixes the length of the *a* axis to be ~4.4 Å. In contradistinction, the monoclinic β angle between the *a* and *c* axes appears to be determined by the requirement of forming close contacts between the ribbons packing along the *a*-axis. This contact distance is indeed equal to the *d*(110) spacing of 3.2 Å.

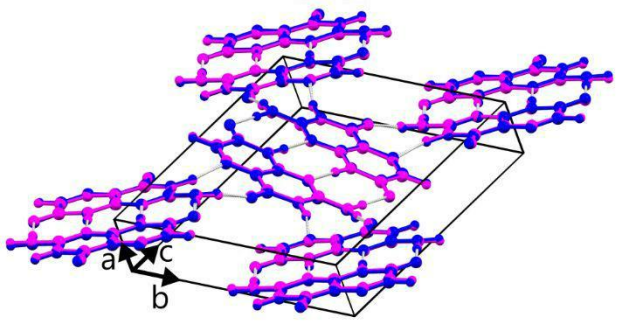

Figure 5 Overlay of the computationally predicted (blue) and experimentally determined (pink) structures for the synthetic isoxanthopterin polymorph.

Table 1 Comparison of structural parameters for the calculated biogenic (β) form and the calculated and Rietveld refined synthetic (α) form of isoxanthopterin. Lattice energy differences (ΔE in kcal/mol, per molecule), calculated using dispersion-augmented DFT, are given relative to that of the β polymorph.

	Biogenic **β** calc.[3]	Synthetic **α** calc.	Synthetic **α** refined
Symmetry	Orthorhombic	Monoclinic	Monoclinic
Space group	*Cmce*	$P12_1/c1$	$P12_1/c1$
a / Å	6.33	4.41	4.48
b / Å	10.72	10.06	9.90
c / Å	19.98	20.15	20.42
β / º	90	130.5	131.2
V / Å^3	1355.4	679.5	682.5
ΔE	0 (ref.)	+0.67	---

Crystal Morphologies

The theoretical growth and equilibrium morphologies of the synthetic α-polymorph of isoxanthopterin were determined using inter-atomic potential energy calculations. The growth analysis predicts a prismatic shape (Figure 6A(i)), elongated in the direction of the short *a*-axis, expressing four dominant {011} faces and two minor {002} side faces. The crystal is terminated at both ends by well-expressed {100} and {102} end faces. Experimentally, the crystal morphology can be characterized by combining electron imaging and diffraction. Representative results for crystals grown from DMSO (Figure 6B-D) had both similarities and differences with the theoretical prediction. Specifically, the observed crystals tend to be prisms, elongated along the short *a*-axis and forming assignable 0*kl* side faces. Some crystals exhibit {020} side faces, despite their absence in the theoretical growth form (see Figure 6B), while other crystals expressed {011} side faces (Figure 6C-D), in agreement with the theoretical growth form. The theoretical growth morphology of the biogenic β-form, Figure 6E(i), is prismatic expressing {111} and {002} faces. By comparison, the calculated equilibrium morphology, Figure 6E(ii), is truncated, expressing {200} faces. Indeed, this morphology is closer to the biogenically observed morphology, which has dominant {200} plate-like faces (presented schematically in Figure 6E(iii)).[3,64]

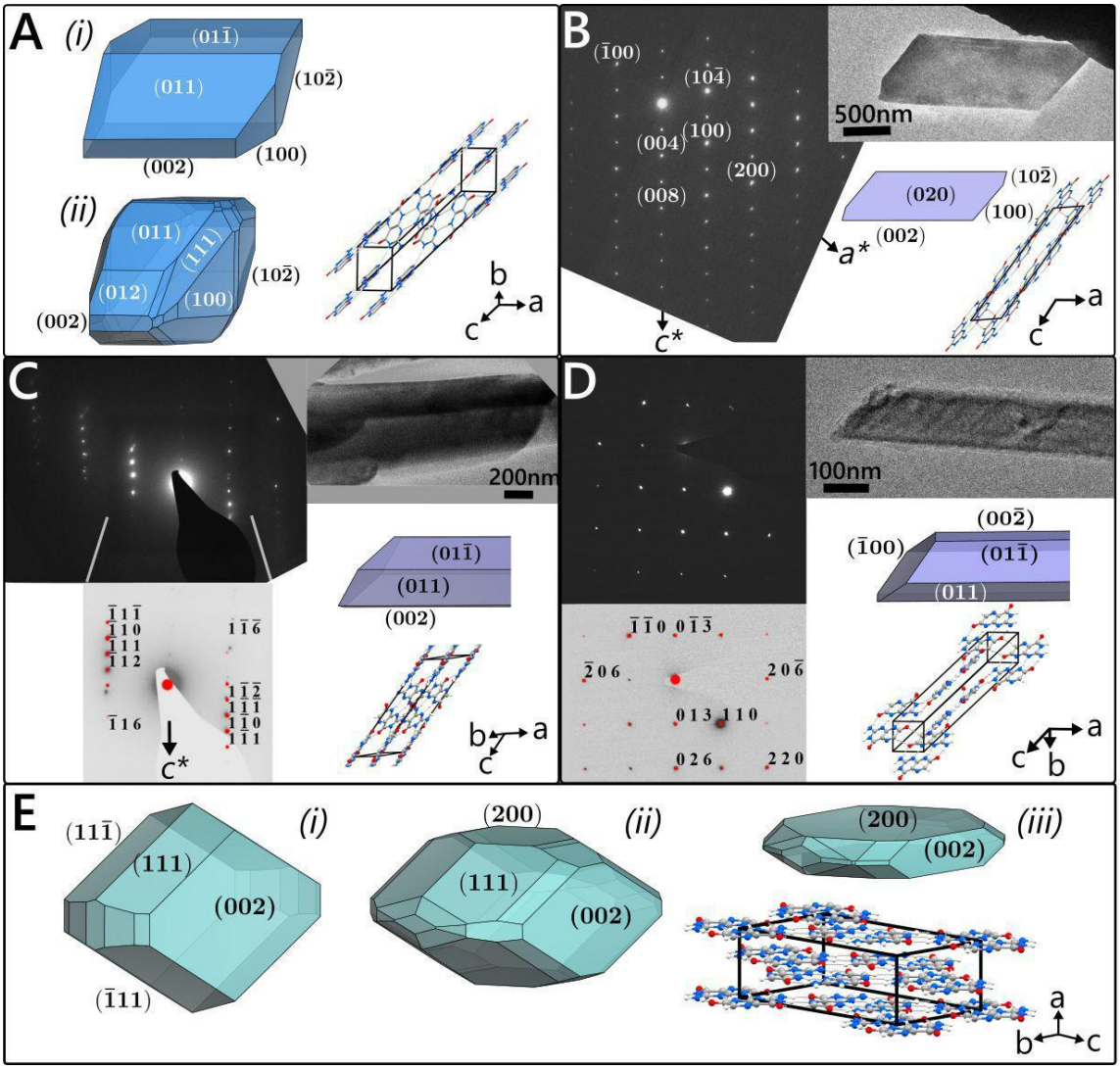

Figure 6 (A-D) Crystal morphology, electron imaging and diffraction of the synthetic α-polymorph of isoxanthopterin. (A) (i): theoretical growth morphology, (ii): equilibrium morphology, and corresponding molecular packing arrangement in the crystal, viewed perpendicular to the (011) plane. (B) Observed *h*0*l* ED pattern and the corresponding crystal. Bottom right: the corresponding molecular packing arrangement, viewed along the *b*-axis and a model of the observed morphology. The crystal exhibits {100} end faces seen edge-on and must lie on the (020) face since the electron beam is parallel to the *b* axis. (C) Measured ED pattern of an *hkl* reflection set and the corresponding crystal shape. Bottom left: Simulated ED pattern - indexed assuming the crystal is mounted along the [110] direction. Bottom right: the corresponding molecular packing arrangement and a model of the crystal shape, which is elongated in the *a*-direction. We deduce from the observed crystal habit and orientation that it exposes (011) and (01
1) side faces. (D) Measured *hkl* ED pattern and corresponding crystal shape. Bottom: Simulated ED pattern, indexed assuming the crystal is mounted along the [331] direction. Bottom right: the corresponding molecular packing arrangement and a model of the needle morphology. The crystal lies almost on the (011) face, which is almost parallel to the [331] direction. (E) Simulated morphologies of biogenic β-isoxanthopterin. (i): theoretical growth form, (ii): computed equilibrium shape, (iii): representative experimental morphology of biogenic β-isoxanthopterin,[3] and corresponding molecular packing arrangement of the crystal.

Refractive index and optical properties

The static macroscopic dielectric tensors of the α- and - polymorphs of isoxanthopterin and guanine were computed using density functional perturbation theory and used to derive principal axial directions and corresponding refractive indices.[65] The resulting refractive indices for the α-polymorph of isoxanthopterin are n_{a^*}=1.43, n_b=1.87, and n_c=1.87. Isoxanthopterin crystals are biaxial, and thus have three different refractive index values, although the refractive indices along the *b* and *c* directions are similar, resulting in almost uniaxial optical properties.

Table 2 Comparison of calculated principal refractive indices (*n*) for the biogenic and synthetic polymorphs of guanine and isoxanthopterin. For orthorhombic isoxanthopterin, the directions of the principal polarization vectors are parallel to the lattice axes. For the monoclinic crystals, one principal optical axis coincides with the unique axis (either *b* or *c*), with the other two principal axes parallel to the *c* or *b* axes, respectively, and the *a** axis, which is perpendicular to the H-bonded *bc* layer.

	Isoxanthopterin		Guanine	
	Synthetic **α** calc.	Biogenic **β** calc.	Synthetic **α** calc.	Biogenic **β** calc.
Symmetry	Monoclinic	Orthorhombic	Monoclinic	Monoclinic
Space group	$P12_1/c1$	*Cmce*	$P12_1/c1$	$P112_1/b$
n_{a^*}	1.43	1.40	1.42	1.43
n_b	1.87	2.02	1.85	1.86
n_c	1.87	1.90	1.89	1.87

IV. Discussion

We first consider the differences and similarities in the molecular packing between the two polymorphs of isoxanthopterin, then correlate them to their physical properties, including crystal morphology and optical reflectivity.

The basic building block for both structures is the H-bonded dimer, which incorporates four H-bonds. In the biogenic β-polymorph, the dimers are interlinked by H-bonds forming layers in the *bc* plane. These (100) layers, as nearest neighbors along the *a* direction, are offset by half a translation along the *b*-axis such that the molecular overlap between

neighboring layers is very limited (Figure 7). Nonetheless, this offset brings about an antiparallel arrangement of both the carbonyl bonds along the *a* axis (a motif that has been observed in a carboxylic acid crystal structure),[66–68] and an NH/π binding motif of the NH_2 group with the pyrazine ring.[69–73]

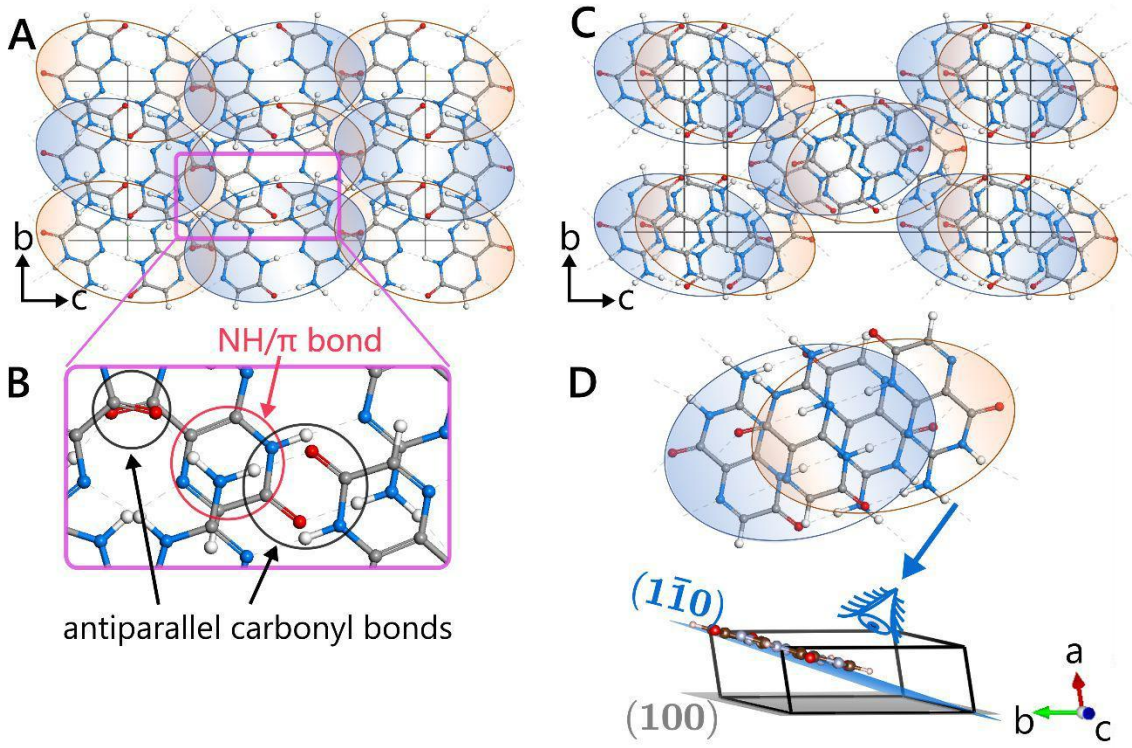

Figure 7 (A) Molecular packing of two neighboring H-bonded layers of biogenic β isoxanthopterin, viewed perpendicular to the layer plane, displaying molecular overlap. (B) A magnified view of A, emphasizing the antiparallel arrangement of C=O carbonyl bonds and the NH/π interaction. (C-D) Molecular packing of two neighboring ribbons of synthetic α-isoxanthopterin related by translation along the short *a* axis; in panel (C) the ribbons are also juxtaposed along the *c* axis to form the unit cell. In (A) and (C) each dimer is highlighted by a colored ellipse; upper dimers in blue, and the lower dimers in orange. (D) The stacking offset between neighboring dimers of synthetic α isoxanthopterin, viewed perpendicular to the dimer plane (1$\bar{1}$0), *i.e.*, perpendicular to the a + b diagonal.

By contrast, the dimers in the synthetic α-polymorph are interlinked via a three-dimensional H-bonded network. This motif is achieved by criss-cross ribbons of the H-bonded dimers, where the ribbons make an angle of 23° with the *bc* plane, and thus a dihedral angle of 46° between juxtaposed ribbons along the *c* axis. As a consequence, the

criss-cross ribbons form out-of-plane NH···O and NH···N bonds. Neighboring parallel ribbons are stacked along the short *a* axis with pronounced overlap.

Interestingly, DFT calculations suggest that the biogenic polymorph of isoxanthopterin is more stable than the synthetic polymorph by 0.7 kcal/mol (see Table 1). However, this difference is still within the overall expected accuracy of the calculation. Therefore, we refrain from commenting on whether the preference for the β-polymorph in the biogenic environment, or the α-polymorph in crystallization from DMSO, is driven by kinetic or thermodynamic factors.

Transparent materials with a high refractive index are of general interest for a wide variety of advanced optical applications.[74–76] As mentioned in the introduction, biogenic isoxanthopterin is predicted to possess an exceptionally high refractive index. It is therefore of interest to compare and contrast the refractive indices of the synthetic and biogenic polymorphs of isoxanthopterin with those of guanine, which is perhaps the prototypical high-refractive index transparent biological material.

The high refractive indices of the isoxanthopterin and guanine crystals in the *bc* plane are determined by the polarizability of the molecule and by the molecular packing in the H-bonded planes. Both the isoxanthopterin polymorphs are formally biaxial, and therefore have three different values of refractive index, but two of which are similar (along the *b* and *c* directions), resulting in almost uniaxial optical properties (Table 2). For the planar -polymorph, the two principal indices within the layer (along the *b* and *c* axes) are similar in magnitude, with an average value n=1.96. For the non-planar α-polymorph, the average value is a slightly lower n=1.87. For both polymorphs, the refractive index along the perpendicular direction is ~1.4. For guanine, the optical properties of the two anhydrous polymorphs are quite similar, which is reasonable in light of the similarity of their structures, with an out-of-plane refractive index of ~1.4 and an average in-plane refractive index of ~1.88 (Table 2). The large anisotropy and the high refractive index along specific directions reported here are consistent with prior work on molecular solids with stacked structures of small organic molecules containing aromatic rings and polar groups.[77]

Previous studies have suggested that the introduction of hetero-aromatic rings containing -C=N-C- bonds, additional polarizable atoms, or electron donating groups on the aromatic rings is expected to increase the refractive index,[78–81] with additional

contributions from hydrogen bonds and sensitivity to the overall packing.[81] Compared to guanine, isoxanthopterin has one additional carbonyl oxygen and has two more H-bonds per molecule (10 for isoxanthopterin; 8 for guanine), which, in all likelihood, contribute to its higher refractive index. The loss of planarity and modification of hydrogen bonding in the synthetic polymorph of isoxanthopterin may explain its somewhat lower refractive index in terms of reduced polarizability. Given the small difference in the refractive indices between the biogenic and synthetic polymorphs, however, it seems unlikely that there will be a significant difference in their optical properties. Consequently, it also seems unlikely that the difference in optical properties between the two polymorphs has determined the preferential evolution of the β polymorph in the biological environment. This evolution is therefore more likely to be due to chemical and physical parameters of the crystallization environment, which are already known to be important in dictating polymorph preference in biomineral systems.[23]

The similarly high values of refractive indices, together with the almost uniaxial properties, make both polymorphs attractive for technological applications such as inexpensive, stable, and biocompatible thin coating layers in optical devices. Optical applications of anisotropic crystals, however, also require control of crystal morphology in order to expose the crystallographic face parallel to the high refractive index plane. For planar isoxanthopterin, the face parallel to the H-bonded layer (*i.e.*, the (100) face) should be exposed. However, the (100) face is expected to be a relatively fast growing direction, and calculation of the theoretical growth morphology yields bulky prisms with small (100) faces.

The crystals of synthetic isoxanthopterin, grown from DMSO, exhibit a common prismatic elongated morphology, with variable side faces developed. The differences between the bulky prismatic growth morphology and the observed needle-like experimental morphology may be rationalized by solvent-crystal surface interactions. The theoretical morphology is based on the crystal structure and symmetry, with the assumption that the relative growth rates of different faces are proportional to their relative attachment energies.[55,57] However, the calculated morphologies do not account for interactions between the growing crystal faces and the solvent (DMSO) environment.[82] A plausible binding motif between the DMSO solvent and the isoxanthopterin molecule would involve

the formation of heterocyclic H-bonded dimers, as shown in Figure 8, akin to that observed in the crystal structure of the β-hematin-DMSO solvate.[83–85] These interactions may occur at the surface of the (0*kl*) faces, thus rationalizing the morphology of the elongated crystals of isoxanthopterin in terms of an interplay between the internal crystal structure and solvent-surface interactions. In contrast to the synthetic α-polymorph, the biogenic crystals of isoxanthopterin develop as thin {100} plates, although the theoretical growth morphology (Figure 6E(i)) is bulky and prismatic, as is the synthetic polymorph.[3,64] The theoretical equilibrium morphology of -isoxanthopterin (Figure 6E(ii)), by comparison, is a truncated prism expressing a pair of {100} faces, which is somewhat closer to the plate-like morphology of the biogenic form (Figure 6E(iii)). How the organism achieves this level of control over crystal morphology is difficult to explain, but it is clear that methods have evolved to achieve the morphology required for the optical function.

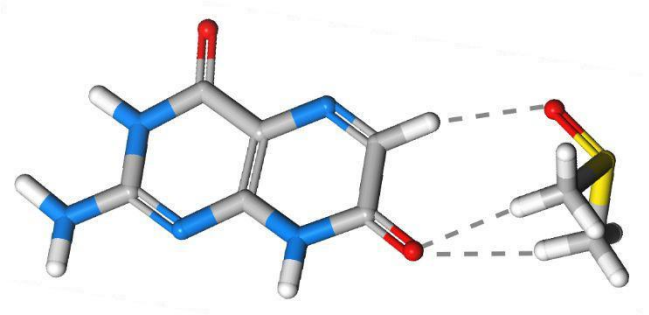

Figure 8 Plausible heterocyclic binding motif of DMSO solvent to the isoxanthopterin molecule at the 0*kl* faces, formed by a C−H···O=S bond and two C−H···O=C bonds as shown. An alternative binding motif is a N−H···O=S bond and two C−H···O=C bonds (not shown).

Analogous to the situation for isoxanthopterin, in the case of guanine-based multilayer reflectors the crystals are found to be very thin and to expose a dominant face parallel to the H-bonded layer.[25,31,86] In contrast, the theoretically-predicted growth morphology is a bulky prism, which is indeed the morphology observed in the white-light scattering crystals found in the white widow spider.[7] Interestingly, crystals grown from water also have a bulky prismatic shape, although the crystal can be induced to form plates using appropriate additives.[87]

Finally, we note that while crystalline guanine is found widely in the reflective systems of animals[7], a pteridine (isoxanthopterin),[3] other purines,[88,89] and even riboflavin[90] have been identified.[12] Especially intriguing is the case of riboflavin (also known as vitamin B2).

This is because the riboflavin molecule has a different structure than the above-discussed planar molecules: it is T-shaped, incorporating three fused heterocyclic rings (an isoalloxazine ring) and a tetrahydroxypentanal side chain. This structure suggests that the molecule cannot form a tightly-packed H-bonded planar layer motif like guanine or biogenic isoxanthopterin. To the best of our knowledge, the structure of crystalline riboflavin has not been reported. However, the fact that the synthetic -polymorph of isoxanthopterin, which embodies a non-planar three-dimensional H-bonded motif, still has a high index of refraction, reinforces the feasibility that biogenic reflecting materials may have a non-planar molecular arrangement.

It follows from the analysis above that an ideal reflective crystal could be designed from a highly polarizable molecule, arranged in a structure that has planar or close-to planar motifs, which endow the material with a high refractive index in the direction parallel to the planar arrangement. If the crystal morphology is such that this plane corresponds to a large plate face, incident light normal to that plane would experience the high refractive index. Synthetic isoxanthopterin appears to pertain to this group of molecules, and can be a convenient candidate for technological applications. If the growth morphology is not suited to the optical requirements, appropriate inhibitors should be designed that will control the crystal morphology in the desired directions.

IV. Conclusions

In conclusion, we have crystallized a synthetic form of isoxanthopterin from DMSO and obtained its crystal structure in two different ways: computationally, entirely from first principles based on a hand-generated packing motif, and independently from powder x-ray diffraction data, using a direct-space genetic algorithm for structure solution followed by Rietveld refinement. The crystal structure is a three-dimensional H-bonded arrangement, different from the planar H-bonded motif of biogenic isoxanthopterin. We have characterized the crystal morphology of the synthetic polymorph both experimentally and theoretically, including consideration of the effect of solvent (DMSO) on the observed morphology *via* solvent surface interactions. In addition, we have computed the refractive indices and found that the dominant refractive indices are slightly lower for the synthetic polymorph of isoxanthopterin than for the biogenic polymorph, but still as high as those of

guanine crystals. Therefore, synthetic isoxanthopterin may be considered as a very promising candidate for incorporation in artificial optical systems.

Supporting Information

Cif file of the structure of the synthetic polymorph, determined directly from PXRD data.

Acknowledgments

We thank Dr. Nadav Elad and Dr. Ronit Popovitz-Biro for their assistance with electron microscopy measurements, Dr. Neta Varsano for scientific discussions and help with related experiments, and Dr. Colan Hughes and Dr. Benson Kariuki for discussions relating to structure determination from PXRD data. We acknowledge the European Synchrotron Radiation Facility for provision of synchrotron radiation facilities and thank Dr. Andy Fitch for assistance in using beamline ID22. This work was supported by Israel Science Foundation Grant 583/ 17. B.A.P. is the recipient of a Human Frontiers Science Program– Cross-Disciplinary Postdoctoral Fellowship. L.A. is the incumbent of the Dorothy and Patrick Gorman Professorial Chair of Biological Ultrastructure. L.K. is the incumbent of the Aryeh and Mintzi Katzman Professorial Chair. B.P acknowledges funding from the European Research Council under the European Union's Seventh Framework Program (FP/2013-2018) / ERC Grant Agreement n. 336077. A.R. gratefully acknowledges support from the Visiting Faculty Program at Weizmann Institute.

REFERENCES

(1) Daubner, S. C.; Fitzpatrick, P. F. Pteridines. In *Encyclopedia of Biological Chemistry (Second Edition)*; Lennarz, W. J., Lane, M. D., Eds.; Academic Press: Waltham, 2013; pp 666–669.

(2) Oliphant, L. W.; Hudon, J. Pteridines as Reflecting Pigments and Components of Reflecting Organelles in Vertebrates. *Pigment Cell Res.* **1993**, *6* (4), 205–208.

(3) Palmer, B. A.; Hirsch, A.; Brumfeld, V.; Aflalo, E. D.; Pinkas, I.; Sagi, A.; Rosenne, S.; Oron, D.; Leiserowitz, L.; Kronik, L.; et al. Optically Functional Isoxanthopterin Crystals in the Mirrored Eyes of Decapod Crustaceans. *PNAS* **2018**, *115* (10), 2299– 2304.

(4) Kleinholz, L. H. Purines and Pteridines from the Reflecting Pigment of the Arthropod Retina. *Biol. Bull.* **1959**, *116* (1), 125–135.

(5) Zyznar, E. S.; Nicol, J. A. C. Ocular Reflecting Pigments of Some Malacostraca. *J. Exp. Mar. Biol. Ecol.* **1971**, *6* (3), 235–248.

(6) Zyznar, E. S.; Nicol, J. A. Reflecting Materials in the Eyes of Three Teleosts, Orthopristes Chrysopterus, Dorosoma Cepedianum and Anchoa Mitchilli. *Proc R Soc Lond B* **1973**, *184* (1074), 15–27.

(7) Gur, D.; Palmer, B. A.; Weiner, S.; Addadi, L. Light Manipulation by Guanine Crystals in Organisms: Biogenic Scatterers, Mirrors, Multilayer Reflectors and Photonic Crystals. *Adv. Funct. Mater.* **2017**, 1603514.

(8) Land, M. F. The Physics and Biology of Animal Reflectors. *Prog. Biophys. Mol. Biol.* **1972**, *24*, 75–106.

(9) Fox, D. L. *Animal Biochromes and Structural Colours: Physical, Chemical, Distributional & Physiological Features of Coloured Bodies in the Animal World*; University of California Press: Berkeley, 1976.
(10) Herring, P. J. Reflective Systems in Aquatic Animals. *Comp. Biochem. Physiol. A Physiol.* **1994**, *109* (3), 513–546.
(11) Palmer, B. A.; Taylor, G. J.; Brumfeld, V.; Gur, D.; Shemesh, M.; Elad, N.; Osherov, A.; Oron, D.; Weiner, S.; Addadi, L. The Image-Forming Mirror in the Eye of the Scallop. *Science* **2017**, *358* (6367), 1172–1175.
(12) Palmer, B. A.; Gur, D.; Weiner, S.; Addadi, L.; Oron, D. The Organic Crystalline Materials of Vision: Structure–Function Considerations from the Nanometer to the Millimeter Scale. *Adv. Mater.* **2018**, *30* (41), 1800006.
(13) Land, M. F. Superposition Images Are Formed by Reflection in the Eyes of Some Oceanic Decapod Crustacea. *Nature* **1976**, *263* (5580), 764.
(14) Schmidt, W. J. Altes Und Neues Über Strukturfarben Im Tierreich. *Giess. Naturwissenschaftliche Vortrage* **1949**, *6*, 1–71.
(15) Panush, S.; Gelmini, J. M. Patent: Subtle Patina Metallic Coatings Containing Guanine. EP0439112A1, July 31, 1991.
(16) Delattre, N.; Thevenet, L. Patent: Cosmetic Composition Comprising White Natural Pigments Having High Coverage. WO2014097134A1, June 26, 2014.
(17) Iwasaka, M.; Miyashita, Y.; Mizukawa, Y.; Suzuki, K.; Toyota, T.; Sugawara, T. Biaxial Alignment Control of Guanine Crystals by Diamagnetic Orientation. *Appl. Phys. Express* **2013**, *6* (3), 037002.
(18) Mizukawa, Y.; Iwasaka, M. Magnetic Control of the Inclination of Biogenic Guanine Crystals Fixed on a Substrate. *J. Appl. Phys.* **2015**, *117* (17), 17B730.
(19) Iwasaka, M.; Mizukawa, Y.; Roberts, N. W. Magnetic Control of the Light Reflection Anisotropy in a Biogenic Guanine Microcrystal Platelet. *Langmuir* **2016**, *32* (1), 180–187.
(20) Lowenstam, H. A.; Weiner, S. *On Biomineralization*; Oxford University Press: New York, 1989.
(21) Mann, S. *Biomineralization: Principles and Concepts in Bioinorganic Materials Chemistry*; Oxford University Press: New York, 2001.
(22) Navrotsky, A. Energetic Clues to Pathways to Biomineralization: Precursors, Clusters, and Nanoparticles. *Proc. Natl. Acad. Sci. U. S. A.* **2004**, *101* (33), 12096–12101.
(23) Cartwright, J. H. E.; Checa, A. G.; Gale, J. D.; Gebauer, D.; Sainz-Díaz, C. I. Calcium Carbonate Polyamorphism and Its Role in Biomineralization: How Many Amorphous Calcium Carbonates Are There? *Angew. Chem. Int. Ed.* **2012**, *51* (48), 11960–11970.
(24) Müller, W. E. G. *Silicon Biomineralization: Biology — Biochemistry — Molecular Biology — Biotechnology*; Springer Science & Business Media: Berlin, Heidelberg, 2012.
(25) Hirsch, A.; Gur, D.; Polishchuk, I.; Levy, D.; Pokroy, B.; Cruz-Cabeza, A. J.; Addadi, L.; Kronik, L.; Leiserowitz, L. "Guanigma": The Revised Structure of Biogenic Anhydrous Guanine. *Chem. Mater.* **2015**, *27* (24), 8289–8297.

(26) Solomonov, I.; Weygand, M. J.; Kjaer, K.; Rapaport, H.; Leiserowitz, L. Trapping Crystal Nucleation of Cholesterol Monohydrate: Relevance to Pathological Crystallization. *Biophys. J.* **2005**, *88* (3), 1809–1817.

(27) Varsano, N.; Fargion, I.; Wolf, S. G.; Leiserowitz, L.; Addadi, L. Formation of 3D Cholesterol Crystals from 2D Nucleation Sites in Lipid Bilayer Membranes: Implications for Atherosclerosis. *J. Am. Chem. Soc.* **2015**, *137* (4), 1601–1607.

(28) Ziblat, R.; Leiserowitz, L.; Addadi, L. Crystalline Lipid Domains: Characterization by X-Ray Diffraction and Their Relation to Biology. *Angew. Chem. Int. Ed.* **2011**, *50* (16), 3620–3629.

(29) Guille, K.; Clegg, W. Anhydrous Guanine: A Synchrotron Study. *Acta Crystallogr. C* **2006**, *62* (8), o515–o517.

(30) Gur, D.; Pierantoni, M.; Dov, N. E.; Hirsh, A.; Feldman, Y.; Weiner, S.; Addadi, L. Guanine Crystallization in Aqueous Solutions Enables Control over Crystal Size and Polymorphism. *Cryst. Growth Des.* **2016**, *16* (9), 4975–4980.

(31) Levy-Lior, A.; Pokroy, B.; Levavi-Sivan, B.; Leiserowitz, L.; Weiner, S.; Addadi, L. Biogenic Guanine Crystals from the Skin of Fish May Be Designed to Enhance Light Reflectance. *Cryst. Growth Des.* **2008**, *8* (2), 507–511.

(32) Fitch, A. N. The High Resolution Powder Diffraction Beam Line at ESRF. *J. Res.-Natl. Inst. Stand. Technol.* **2004**, *109*, 133–142.

(33) Harris, K. D. M. Powder Diffraction Crystallography of Molecular Solids. In *Advanced X-Ray Crystallography*; Rissanen, K., Ed.; Topics in Current Chemistry; Springer Berlin Heidelberg: Berlin, Heidelberg, 2012; pp 133–177.

(34) Werner, P. E.; Eriksson, L.; Westdahl, M. TREOR, a Semi-Exhaustive Trial-and-Error Powder Indexing Program for All Symmetries. *J. Appl. Crystallogr.* **1985**, *18* (5), 367–370.

(35) Shirley, R. *The Crysfire 2002 System for Automatic Powder Indexing: User's Manual*; The Lattice Press: Guildford, 2002.

(36) Le Bail, A.; Duroy, H.; Fourquet, J. L. Ab-Initio Structure Determination of LiSbWO6 by X-Ray Powder Diffraction. *Mater. Res. Bull.* **1988**, *23* (3), 447–452.

(37) Larson, A. C.; Von Dreele, A. B. "General Structure Analysis System (GSAS). *Los Almos Natl. Lab. Rep. LAUR* **2004**, 86–748.

(38) Kariuki, B. M.; Serrano-González, H.; Johnston, R. L.; Harris, K. D. M. The Application of a Genetic Algorithm for Solving Crystal Structures from Powder Diffraction Data. *Chem. Phys. Lett.* **1997**, *280* (3), 189–195.

(39) Kariuki, B. M.; Calcagno, P.; Harris, K. D. M.; Philp, D.; Johnston, R. L. Evolving Opportunities in Structure Solution from Powder Diffraction Data—Crystal Structure Determination of a Molecular System with Twelve Variable Torsion Angles. *Angew. Chem. Int. Ed.* **1999**, *38* (6), 831–835.

(40) Harris, K. D. M.; Habershon, S.; Cheung, E. Y.; Johnston, R. L. Developments in Genetic Algorithm Techniques for Structure Solution from Powder Diffraction Data. *Z. Für Krist. - Cryst. Mater.* **2004**, *219* (12), 838–846.

(41) Albesa-Jové, D.; Kariuki, B. M.; Kitchin, S. J.; Grice, L.; Cheung, E. Y.; Harris, K. D. M. Challenges in Direct-Space Structure Determination from Powder Diffraction Data: A Molecular Material with Four Independent Molecules in the Asymmetric Unit. *ChemPhysChem* **2004**, *5* (3), 414–418.

(42) Williams, P. A.; Hughes, C. E.; Harris, K. D. M. L-Lysine: Exploiting Powder X-Ray Diffraction to Complete the Set of Crystal Structures of the 20 Directly Encoded Proteinogenic Amino Acids. *Angew. Chem. Int. Ed.* **2015**, *54* (13), 3973–3977.
(43) Hughes, C. E.; Manjunatha Reddy, G. N.; Masiero, S.; P. Brown, S.; Andrew Williams, P.; M. Harris, K. D. Determination of a Complex Crystal Structure in the Absence of Single Crystals: Analysis of Powder X-Ray Diffraction Data, Guided by Solid-State NMR and Periodic DFT Calculations, Reveals a New 2′-Deoxyguanosine Structural Motif. *Chem. Sci.* **2017**, *8* (5), 3971–3979.
(44) Clark, S. J.; Segall, M. D.; Pickard, C. J.; Hasnip, P. J.; Probert, M. I. J.; Refson, K.; Payne, M. C. First Principles Methods Using CASTEP. *Z. Für Krist. - Cryst. Mater.* **2009**, *220* (5/6), 567–570.
(45) Perdew, J. P.; Burke, K.; Ernzerhof, M. Generalized Gradient Approximation Made Simple. *Phys. Rev. Lett.* **1996**, *77* (18), 3865–3868.
(46) Tkatchenko, A.; Scheffler, M. Accurate Molecular Van Der Waals Interactions from Ground-State Electron Density and Free-Atom Reference Data. *Phys. Rev. Lett.* **2009**, *102* (7), 073005.
(47) Kresse, G.; Hafner, J. *Ab Initio* Molecular Dynamics for Liquid Metals. *Phys. Rev. B* **1993**, *47* (1), 558–561.
(48) Al-Saidi, W. A.; Voora, V. K.; Jordan, K. D. An Assessment of the VdW-TS Method for Extended Systems. *J. Chem. Theory Comput.* **2012**, *8* (4), 1503–1513.
(49) Bučko, T.; Lebègue, S.; Hafner, J.; Ángyán, J. G. Tkatchenko-Scheffler van Der Waals Correction Method with and without Self-Consistent Screening Applied to Solids. *Phys. Rev. B* **2013**, *87* (6), 064110.
(50) Kresse, G.; Joubert, D. From Ultrasoft Pseudopotentials to the Projector Augmented-Wave Method. *Phys. Rev. B* **1999**, *59* (3), 1758–1775.
(51) Baroni, S.; Resta, R. *Ab Initio* Calculation of the Macroscopic Dielectric Constant in Silicon. *Phys. Rev. B* **1986**, *33* (10), 7017.
(52) Gajdoš, M.; Hummer, K.; Kresse, G.; Furthmüller, J.; Bechstedt, F. Linear Optical Properties in the Projector-Augmented Wave Methodology. *Phys. Rev. B* **2006**, *73* (4), 045112.
(53) Momma, K.; Izumi, F. VESTA 3 for Three-Dimensional Visualization of Crystal, Volumetric and Morphology Data. *J. Appl. Crystallogr.* **2011**, *44* (6), 1272–1276.
(54) Hartman, P.; Bennema, P. The Attachment Energy as a Habit Controlling Factor: I. Theoretical Considerations. *J. Cryst. Growth* **1980**, *49* (1), 145–156.
(55) Docherty, R.; Clydesdale, G.; Roberts, K. J.; Bennema, P. Application of Bravais-Friedel-Donnay-Harker, Attachment Energy and Ising Models to Predicting and Understanding the Morphology of Molecular Crystals. *J. Phys. Appl. Phys.* **1991**, *24* (2), 89.
(56) Abbona, F.; Aquilano, D. Morphology of Crystals Grown from Solutions. In *Springer Handbook of Crystal Growth*; Dhanaraj, G., Byrappa, K., Prasad, V., Dudley, M., Eds.; Springer Handbooks; Berlin, Heidelberg, 2010; pp 53–92.
(57) Berkovitch-Yellin, Z. Toward an Ab Initio Derivation of Crystal Morphology. *J. Am. Chem. Soc.* **1985**, *107* (26), 8239–8253.
(58) Fiorentini, V.; Methfessel, M. Extracting Convergent Surface Energies from Slab Calculations. *J. Phys. Condens. Matter* **1996**, *8* (36), 6525.

(59) Mayo, S. L.; Olafson, B. D.; Goddard, W. A. DREIDING: A Generic Force Field for Molecular Simulations. *J. Phys. Chem.* **1990**, *94* (26), 8897–8909.
(60) Brown, E. G. Pteridines. In *Ring Nitrogen and Key Biomolecules: The biochemistry of N-heterocycles*; Brown, E. G., Ed.; Springer Netherlands: Dordrecht, 1998; pp 167–179.
(61) Desiraju, G.; Steiner, T. *The Weak Hydrogen Bond: In Structural Chemistry and Biology*; International Union of Crystallography Monographs on Crystallography; Oxford University Press: New York, 2001.
(62) Berkovitch-Yellin, Z.; Leiserowitz, L. The Role Played by C–H···O and C–H···N Interactions in Determining Molecular Packing and Conformation. *Acta Crystallogr. Sect. B* **1984**, *40* (2), 159–165.
(63) Bernstein, J.; Cohen, M. D.; Leiserowitz, L. The Structural Chemistry of Quinones. In *Quinonoid Compounds*; John Wiley & Sons, Inc: London, 1974; Vol. 1, pp 37–110.
(64) Benjamin A. Palmer *et al. Submitted for Publication*.
(65) Saleh, B. E. A.; Teich, M. C. Polarization and Crystal Optics. In *Fundamentals of Photonics*; John Wiley & Sons, Inc.: New York, 1991; pp 193–237.
(66) Miller, R. S.; Curtin, D. Y.; Paul, I. C. Reactions of Molecular Crystals with Gases. III. Relation of Anisotropy to Crystal Structure in Reactions of Carboxylic Acids and Anhydrides with Ammonia Gas. *J. Am. Chem. Soc.* **1974**, *96* (20), 6340–6349.
(67) Leiserowitz, L. Molecular Packing Modes. Carboxylic Acids. *Acta Crystallogr. Sect. B* **1976**, *32* (3), 775–802.
(68) Berkovitch-Yellin, Z.; Leiserowitz, L. Atom-Atom Potential Analysis of the Packing Characteristics of Carboxylic Acids. A Study Based on Experimental Electron-Density Distributions. *J. Am. Chem. Soc.* **1982**, *104* (15), 4052–4064.
(69) Rodham, D. A.; Suzuki, S.; Suenram, R. D.; Lovas, F. J.; Dasgupta, S.; Goddard Iii, W. A.; Blake, G. A. Hydrogen Bonding in the Benzene–Ammonia Dimer. *Nature* **1993**, *362* (6422), 735–737.
(70) Duan, G.; Smith, V. H.; Weaver, D. F. An Ab Initio and Data Mining Study on Aromatic–Amide Interactions. *Chem. Phys. Lett.* **1999**, *310* (3), 323–332.
(71) Imai, Y. N.; Inoue, Y.; Nakanishi, I.; Kitaura, K. Amide–π Interactions between Formamide and Benzene. *J. Comput. Chem.* **2009**, *30* (14), 2267–2276.
(72) Wheeler, S. E.; Bloom, J. W. G. Toward a More Complete Understanding of Noncovalent Interactions Involving Aromatic Rings. *J. Phys. Chem. A* **2014**, *118* (32), 6133–6147.
(73) Bootsma, A. N.; Wheeler, S. E. Stacking Interactions of Heterocyclic Drug Fragments with Protein Amide Backbones. *ChemMedChem* **2018**, *13* (8), 835–841.
(74) Zerbi, G. *Organic Materials for Photonics: Science and Technology*; European Materials Research Society monographs ; Volume 6; North Holland: Amsterdam, 1993.
(75) Higashihara, T.; Ueda, M. Recent Progress in High Refractive Index Polymers. *Macromolecules* **2015**, *48* (7), 1915–1929.
(76) Bosshard, C.; Hulliger, J.; Florsheimer, M.; Gunter, P. *Organic Nonlinear Optical Materials*; Gordon and Breach Science Publication: Amsterdam, 1995.

(77) Jayatilaka, D.; Munshi, P.; J. Turner, M.; K. Howard, J. A.; A. Spackman, M. Refractive Indices for Molecular Crystals from the Response of X-Ray Constrained Hartree–Fock Wavefunctions. *Phys. Chem. Chem. Phys.* **2009**, *11* (33), 7209–7218.
(78) Osaheni, J. A.; Jenekhe, S. A.; Perlstein, J. Photogeneration of Charge Carriers in Bilayer Assemblies of Conjugated Rigid-Rod Polymers. *J. Phys. Chem.* **1994**, *98* (48), 12727–12736.
(79) Yang, C. J.; Jenekhe, S. A. Effects of Structure on Refractive Index of Conjugated Polyimines. *Chem. Mater.* **1994**, *6* (2), 196–203.
(80) Bertarelli, C.; Bianco, A.; D'Amore, F.; Gallazzi, M. C.; Zerbi, G. Effect of Substitution on the Change of Refractive Index in Dithienylethenes: An Ellipsometric Study. *Adv. Funct. Mater.* **2004**, *14* (4), 357–363.
(81) Dos Santos, L.; Macchi, P.; Dos Santos, L. H. R.; Macchi, P. The Role of Hydrogen Bond in Designing Molecular Optical Materials. *Crystals* **2016**, *6* (4), 43.
(82) Weissbuch, I.; Popovitz-Biro, R.; Lahav, M.; Leiserowitz, L. Understanding and Control of Nucleation, Growth, Habit, Dissolution and Structure of Two- and Three-Dimensional Crystals Using "Tailor-Made" Auxiliaries. *Acta Crystallogr. Sect. B* **1995**, *51* (2), 115–148.
(83) Lahav, M.; Leiserowitz, L. A Stereochemical Approach That Demonstrates the Effect of Solvent on the Growth of Polar Crystals: A Perspective. *Cryst. Growth Des.* **2006**, *6* (3), 619–624.
(84) Gildenhuys, J.; Roex, T. le; Egan, T. J.; de Villiers, K. A. The Single Crystal X-Ray Structure of β-Hematin DMSO Solvate Grown in the Presence of Chloroquine, a β-Hematin Growth-Rate Inhibitor. *J. Am. Chem. Soc.* **2013**, *135* (3), 1037–1047.
(85) Straasø, T.; Marom, N.; Solomonov, I.; Barfod, L. K.; Burghammer, M.; Feidenhans'l, R.; Als-Nielsen, J.; Leiserowitz, L. The Malaria Pigment Hemozoin Comprises at Most Four Different Isomer Units in Two Crystalline Models: Chiral as Based on a Biochemical Hypothesis or Centrosymmetric Made of Enantiomorphous Sectors. *Cryst. Growth Des.* **2014**, *14* (4), 1543–1554.
(86) Hirsch, A.; Palmer, B. A.; Elad, N.; Gur, D.; Weiner, S.; Addadi, L.; Kronik, L.; Leiserowitz, L. Biologically Controlled Morphology and Twinning in Guanine Crystals. *Angew. Chem. Int. Ed.* **2017**, *56* (32), 9420–9424.
(87) Gur, D.; Addadi, L.; Weiner, S. Patent: Synthetic Co-Crystals of Anhydrous Guanine and Process for Preparing the Same. WO2017221245A1, December 28, 2017.
(88) Caveney, S. Cuticle Reflectivity and Optical Activity in Scarab Beetles: The Role of Uric Acid. *Proc. R. Soc. Lond. B Biol. Sci.* **1971**, *178* (1051), 205–225.
(89) Böhm, A.; Pass, G. The Ocelli of Archaeognatha (Hexapoda): Functional Morphology, Pigment Migration and Chemical Nature of the Reflective Tapetum. *J. Exp. Biol.* **2016**, *219*, 3039–3048.
(90) Pirie, A. Crystals of Riboflavin Making up the Tapetum Lucidum in the Eye of a Lemur. *Nature* **1959**, *183* (4666), 985.